Polymer 51 (2010) 3989–3997

Contents lists available at ScienceDirect

Polymer

journal homepage: www.elsevier.com/locate/polymer

Structure property correlations for electrospun nanofiber nonwovens

D. Hussain, F. Loyal, A. Greiner, J.H. Wendorff*

Department of Chemistry and Center of Material Science, Philipps-University Marburg, Hans-Meerwein-Str., D-35032 Marburg, Lahn, Germany

ARTICLE INFO

Article history:
Received 22 April 2010
Received in revised form
16 June 2010
Accepted 18 June 2010
Available online 26 June 2010

Keywords:
Pore size
Permeation
Surface area

ABSTRACT

Highly porous nonwovens composed of nanofibers and produced by electrospinning are key elements in a broad range in technical but also in Life Science areas. Applications for gas or fluid filtration, textile applications, carriers for catalysts and scaffolds for tissue engineering are selected examples. These applications require well defined nonwoven parameters such as in particular pore diameters, internal surfaces as well as permeation properties. Electrospinning, on the other hand, allows to control structural parameters such as fiber diameter, nonwoven architecture as well as in certain limits the total porosity. It is thus highly important to know as much as possible about the correlations between the structural parameters controlled by electrospinning and the parameters controlling the performance of the nonwovens composed of the electrospun nanofibers. In the present contribution we analyze these correlations for different types of electrospun nonwovens for a broad range of fiber diameters on an experimental scale The nonwoven considered are composed of polyacrylonitrile (PAN) and polyamide 6 (PA 6) fibers. Results are that pore diameters, specific surface area and permeation coefficients scale in a transparent way with fiber diameters. Finally we briefly compare these experimental results with corresponding predictions gained for ideal nonwovens predominantly from Monte Carlo simulations. The results suggest that one is able to design electrospun nanofiber based nonwovens with predetermined properties and functions in a highly controlled way.

1. Introduction

Nonwovens composed of polymer nanofibers and produced via electrospinning are meeting currently with an ever increasing attention in a broad range of applications involving both technical and Life Science directions. Prominent examples for advanced types of applications for such nonwovens are highly effective and selective filters for gases, fluids or aerosols, carriers for homogeneous or heterogeneous catalysts and inlets or surface membranes for textiles introducing strong wind protections, antibacterial functions and even self-cleaning effects. Further applications include highly porous scaffolds for tissue engineering able to enhance cell proliferation, differentiation or guiding cell growth along specific directions [1–8]. Fundamental requirements in all cases introduced above refer to well controlled pore sizes, enhanced specific surface areas and to precisely defined permeation properties. Frequently one also may have to induce specified nonwoven architectures including uniaxial, planar or three-dimensionally random fiber orientations. The pore sizes will control among others the sizes of solid particles or aerosols to be filtered out but also the depth growth of cells in scaffolds or the wind protection efficiency. The specific surface areas will affect, for instance, the catalytic efficiency or the binding of cells to the fibers and thus to scaffolds composed of them. To design nonwoven components for particular kind of applications one has to be able to control the characteristic nonwoven features introduced above, in particular pore sizes, internal surfaces, permeation properties.

In fact, the parameters which are primarily controlled in the electrospinning process are fiber diameter, porosity to a certain extent and, of course, also the orientational order of the fibers deposited via the electrospinning process. It is known, for instance, that principal parameters which can be exploited to control fiber diameters are the polymer concentration in the spinning solution or the feeding rate, yet the applied field or the distance between the spinning die and the counter electrode are also parameters which might be used to control fiber diameters [2,3,5,7,8]. The total porosity may be varied via modifications of the solvent composition, of the temperature of the spinning solutions yielding wet fibers on deposition but also via modifications of the cross-sectional geometry of the fibers such as the ones causing ribbon-type fibers [9–18]. The specific surface finally may be changed via the introduction of pores in the fibers or of beads, barbs along the fibers and the nonwoven architecture can be affected by the counter electrode configurations chosen, as obvious from detailed studies published in the literature [6,8,19–23].

* Corresponding author.
E-mail address: wendorff@staff.uni-marburg.de (J.H. Wendorff).

0032-3861/$ – see front matter © 2010 Elsevier Ltd. All rights reserved.
doi:10.1016/j.polymer.2010.06.036

The fundamental problem which obviously has thus to be solved in nonwoven designs is the analysis of the correlation between the primary parameters which are directly controlled in electrospinning and the secondary parameters which define the performance of the nonwovens. This is the topic which is addressed in the present paper based predominantly on experimental investigations.

In fact, theoretical studies both analytical ones and simulations exist which were motivated in the context of classical nonwovens composed of fibers with diameters well in the 10 μm range. They aim at applications in filters or textiles and they have proven themselves to be extremely helpful for nonwoven designs. The predictions of such theoretical studies tend to be displayed in reduced quantities – i.e. scaling with the fiber diameters – so that the predictions might, in principle, be adapted to a significant extent directly also to nonwovens prepared from nanofibers [24–26]. The drawback of such simulations, as far as predictions on structure property correlations in electrospun nanofiber nonwovens is concerned, is that ideal model nonwovens characterized by strictly linear fibers with uniform diameter and smooth surfaces are considered.

Electrospinning on the other hand results in nonwovens with various well defined degrees of nonidealities which in turn control application oriented properties. It was thus important to analyze their structure property correlations in detail on an experimental basis. In fact, we will tentatively make a brief effort at the end of the paper to compare these results with predictions from simulations performed for ideal nonwovens. The final goal is to be able to propose reliable procedures for the design and control of electrospun nanofibers nonwovens taking experimental and to a certain extent theoretical concepts into account.

2. Experimental

2.1. Preparation of model nonwovens

To prepare the nonwovens a conventional electrospinning set-up used was composed of syringe type dies attached to a solution feeding pump unit. The applied voltage was about 15 kV with a distance between the die electrode and the counter electrode amounting to about 20 cm. Details of this set-up have been reported previously [1,3,8]. To prepare nonwovens with a bimodal distribution of the fiber diameters we employed a multiple syringe type set-up – four dies – as reported previously feeding two different kinds of polymer solutions – here with respect to the polymer concentrations – through the dies [27].

We investigated first of all nanofiber nonwovens made from polyacrylonitrile (PAN) using *N,N*-dimethylformamide (DMF) as solvent. PAN fibers tend to show circular cross-sections for all fiber diameters. To achieve fibers with various diameters in the range from about 150 nm up to 1.3 μm we varied the polymer concentrations in the spinning solutions. These variations amounted to 7–14 w% in the case of PAN.

We investigated furthermore nanofiber nonwovens made from polyamide 6 (PA 6) using formic acid as solvent. To achieve fibers with various diameters in the range from about 150 nm up to 2.0 μm we varied the polymer concentrations in the spinning solutions. These variations amounted to 15–35 w% in the case of PA 6. PA 6 nanofibers are known to show a strong tendency towards ribbon formation at intermediate concentrations of spinning solutions the origin of such particular shape still being a matter of discussion [8]. The formation of ribbon-type nanofibers via electrospinning was achieved here by selecting PA 6 spinning solutions in the concentration range between 27.5 and 32.5 w% in formic acid.

The architecture of the nonwovens was analysed using a SEM (JSM-7500F, JEOL). The total porosity was determined by measuring the total volume of a given piece of nonwoven geometrically as well as from its weight.

2.2. Analysis of pore sizes

It is important to point out that the pores characteristic of electrospun nonwovens differ strongly from pores with circular cross-sectional areas. Polygon shaped pores are defined in nonwovens by intersections of the nanofibers as illustrated in particular in Fig. 1 showing a top down view on the planar nonwoven (x,y plane). The transport of fluids, gases takes place in the nonwovens considered here along the normal of this plane i.e. along the *z*-direction.

To determine the geometric pore sizes of such nonwovens we embedded the nonwovens in an epoxy matrix and performed cuts after the solidification of the embedded nonwoven along the *z*-direction revealing thus the *z–x* plane which also corresponds to the *z–y* planes for the planar isotropic nonwovens considered here. The fiber ends are well distinguished from the matrix as obvious from Fig. 2. The cross-sections are – as particularly obvious in Fig. 2a – either circular or elliptically elongated as expected for a cut through fibers with various orientations in the nonwoven. Very similar images are available from the Monte Carlo simulations presented in the literature [26]. The distances between one fiber end and the next one along a given direction in the plane – i.e. the intersection length – was determined in the next step for various locations in the plane and for different directions and this was done for different cuts. This procedure allowed to determine the average pore size within the *z–x* or *z–y* planes for that matter as well as the anisotropy of the pore sizes with respect to the *z*-directions. The general finding is that the pores tend to be larger in the *x* or *y* direction relative to the *z*-direction by about 10%. These data are displayed and discussed in the following part of the paper concerned with experimental results.

The onset of the flow of gases through a nonwoven filled with wetting liquids (wet nonwoven) is not directly controlled by the geometric pore sizes but rather by the size of so-called capillary pores which pass in an irregular fashion from one side of the nonwoven to the other one. To obtain data on this quantity the

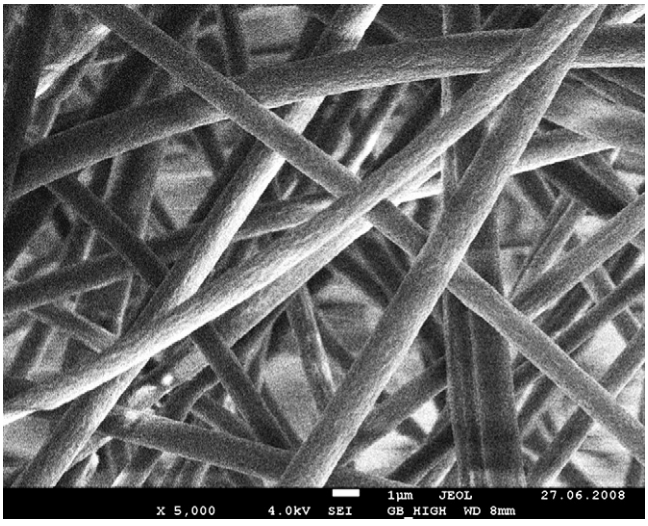

Fig. 1. Top down view on planar nonwoven (*x*, *y* plane) with the transport of fluids, gases taking place along the normal of this plane i.e. along the *z*-direction (Example: nonwoven composed of PAN nanofibers, see also Fig. 4c).

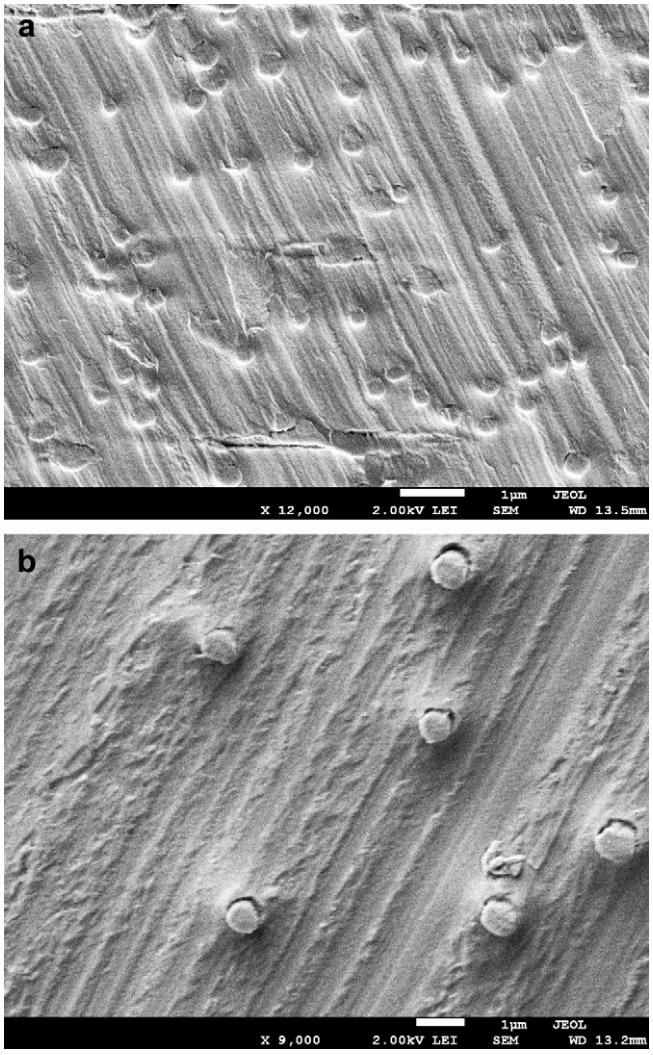

Fig. 2. Cross-section of PAN nonwovens embedded in an epoxy matrix, a) fiber diameter 309 nm, b) fiber diameter 520 nm.

capillary flow porometry technique can be applied [28,29]. We used for this purpose a capillary flow porometer (CFP 1200-AEXL, PMI). The first step of the analysis consists in applying different magnitudes of pressure gradient to a dry nonwoven membrane and to determine the flow of gas through the membrane yielding the so-called dry curve (Fig. 3, upper curve). Next the membrane is immersed completely in wetting liquid (here: Galwick™), so that all pores are completely filled. Again a pressure gradient is applied yet no gas flow is possible unless a critical pressure gradient is surpassed (Fig. 3, lower curve). The reason is that capillary forces scaling inversely with the pore diameters counteract the effect of the pressure gradient. Gas flow can set in only if the effect of the pressure gradient surpasses the one of the capillary forces. The onset of gas flow allows to calculate the diameter of the capillary pore with the largest diameter, called bubble point pore in the following. Finally if the pressure gradient is high enough even the smallest capillary pores can contribute to the gas flow and the so-called wet curve approaches the one of the dry nonwoven discussed above. The pressure gradient for which this happens allows to calculate the diameter of the smallest capillary pores and in principle from the differences between the wet and the dry curve one is able to calculate also the pore size distribution and the average pore size (mean flow pore size) discussed here.

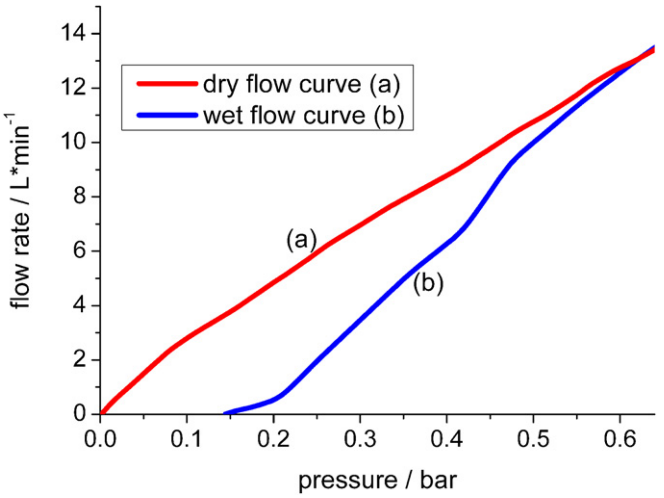

Fig. 3. Dry (upper curve) and wet flow (lower curve) characteristics of a nonwoven as determined by capillary flow porometry. The fiber diameter is 520 nm.

Again selected results will be discussed in the following part of this paper. It should be pointed out here that no theoretical approach is known able to relate the dimensions of capillary pores and geometric pores as defined above on an absolute scale.

To determine the internal specific surface of the nonwovens we used the BET technique well documented in the literature [30]. For this purpose we employed two different commercial set-ups, i.e. Micromeritics Gemini V, Micromeritics Instruments Corp. and BELSOPR-mini II, BEL JAPAN, Inc..

Finally the permeation coefficient k was determined. The analysis was based on the Darcy law

$$u(x) = \frac{-k}{\eta}\nabla p(x)$$

with $u(x)$ being the flux, η the viscosity, $\nabla p(x)$ the pressure gradient and k the permeation coefficient We used the dry curve as available from the capillary flow porometry and as displayed above in Fig. 3 to determine it.

3. Results and discussions

The organization of this part is as follows. To begin with nonwovens composed of PAN fibers with circular cross-sectional geometry as electrospun from solutions in dimethylformamide are discussed characterized by a uniform average fiber diameter which is of course subjected to a certain diameter distribution. The second type of nonwovens to be discussed here is characterized by a bimodal fiber diameter distribution based on PAN fibers again spun from dimethylformamide. Finally the third kind of nonwoven to be considered is composed of nanofibers produced from a solution of PA 6 in formic acid where the spinning conditions are chosen such that flat fibers i.e. ribbon-shaped fibers are produced.

3.1. Nonwoven with unimodal fiber diameter distribution

Nonwovens were prepared from PAN fibers using spinning solutions with different PAN concentrations to produce fibers with different average diameters. Fig. 4a–c displays selected examples of PAN nonwovens with three different magnitudes for the fiber diameter ranging from about 150 to about 1300 nm. Polygon shaped pores are obvious in all cases. Fig. 4d displays the variation of the fiber diameter with the polymer concentration used for the

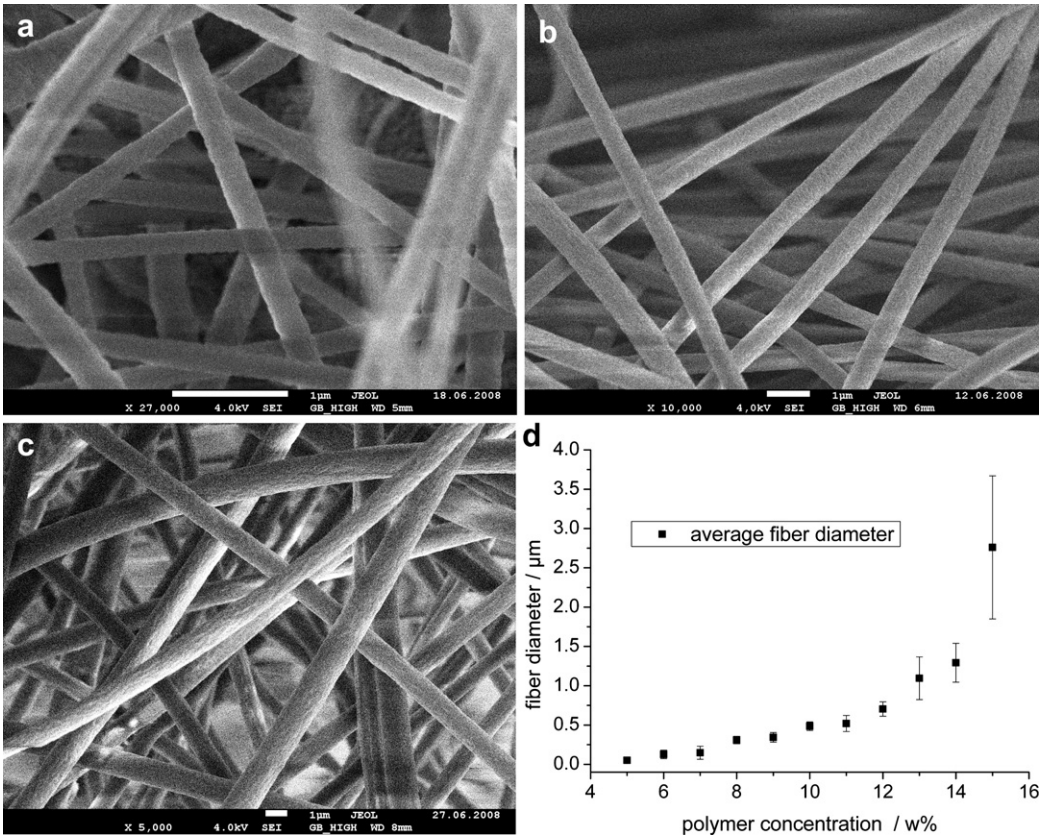

Fig. 4. Nonwovens composed of PAN nanofiber with different fiber diameters a) 148 nm, b) 520 nm, c) 1095 nm, d) variation of diameter with polymer concentration in spinning solution.

spinning solution. It is quite obvious first of all that the polymer concentration in the spinning solution can be used to tailor the fiber diameter. It ranges from about 150 nm up to about 3000 nm in the case considered here. It is furthermore obvious that the fiber diameter is subjected to a certain distribution as also displayed in Fig. 4d via the error bars. Finally it is qualitatively evident by visual inspection that the pore sizes defined by the fibers acting as boundaries increase as the fiber diameters are increased as expected from theory but also geometric arguments.

Using geometrical volume determination for a given piece of nonwoven as well as its weight we determined the total porosity ϵ of the nonwovens as detailed above in the experimental section. This value turned out to be about 0.85 ± 0.02 independent of the fiber diameter considered.

The key feature controlling among other filter performances etc. is the pore structure in particular the size of the pores. Using cross-sectional cuts of nonwovens imbedded in an epoxy matrix already discussed above allowed to determine the average geometric pore diameter as a function of the average fiber diameter. This dependence is displayed in Fig. 5a. It is obvious despite a significant scattering of the data points that the pore diameter increases to a good approximation in a linear fashion with the diameter of the fibers. A second approach towards characterizing the pore structure consists in the determination of the diameter of the capillary pores as determined by capillary flow porometry. The results are displayed in Fig. 5b.

Again the pore diameters – bubble point pores, mean flow pores – increase in a nearly linear way with the fiber diameters over a range of diameters varying by more than one order of magnitude. On the average the ratio of the geometric pore size (diameter) to the fiber diameter amounts to about 6 whereas it assumes values of about 5 for the mean capillary pore size (mean flow pore size) and about 9 for the largest capillary pore size (bubble point pore size). The geometric pore sizes are thus within the range defined by the largest and the average capillary pore diameters.

A further important feature controlling filter performance is the specific surface area as discussed above. This quantity was determined experimentally using the BET technique. The experimental results are displayed in Fig. 6 as function of the fiber diameters. From purely geometric arguments one expects that the specific surface area scales with the inverse of the fiber diameter (red data points) and this is what is also apparent from the experimental BET-results (black data points) shown in Fig. 6. The experimental values are in the range from about 40 m^2/g to 2 m^2/g as the fiber diameter is increased from about 150 nm to 1.3 μm. It seems that on the average the experimental points are slightly higher than the ones calculated on the basis of geometric arguments. One reason certainly is that the surface of the fibers is not ideally smooth as apparent from Fig. 7. We will come back to this finding below in more detail.

Finally the permeation properties will be discussed. The gas flow through the nonwoven (perpendicular to nonwoven planes) as a function of the pressure drop can be analyzed using the capillary flow porometer introduced above. Fig. 8 reveals that the gas flow increases roughly linearly with increasing pressure drop and that it increases at constant pressure drop as the fiber diameters increase.

These results i.e. increase of gas flow with increasing pressure drop and fiber radii are expected at least on a qualitative way. These data can be used following the Darcy law (see above) to calculate first of all the permeation coefficient k. It turned out to be in the range from 1×10^{-14} to 9×10^{-14} m^2 for the nonwovens considered here. Secondly these flow curves allow to determine the

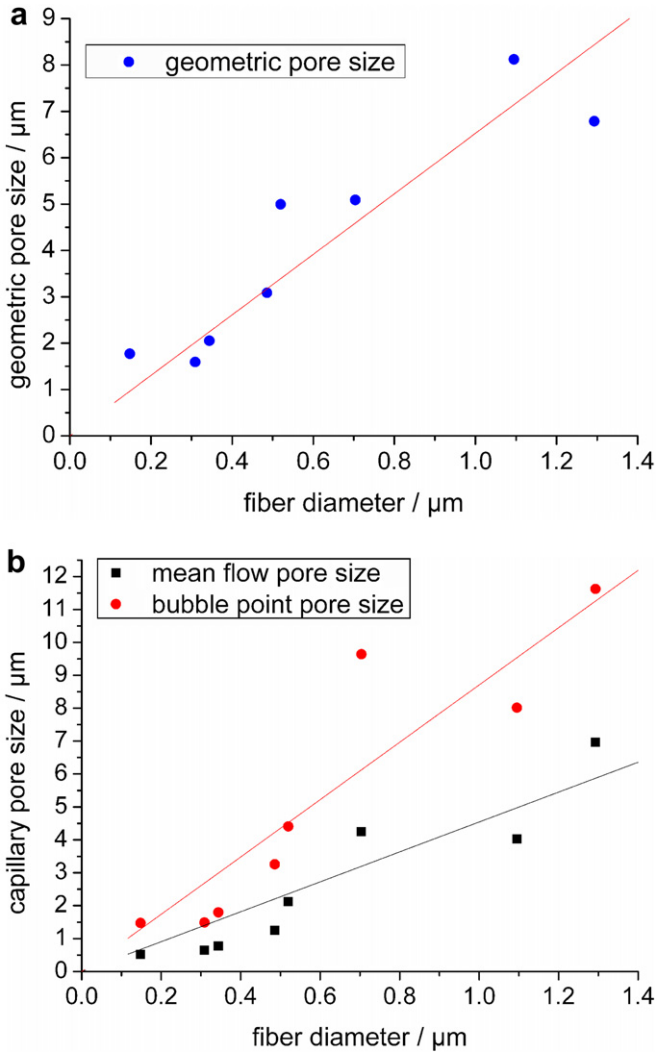

Fig. 5. Dependence of pore diameters on fiber diameters for PAN – based nonwovens a) geometric pore size; b) capillary pore sizes, largest pore sizes (bubble point pores), average pore sizes (mean flow pores).

corresponding reduced quantity k/r^2 (r: radius of fibers) of the permeation coefficient as obtained by dividing all permeation values by the square of the corresponding fiber radius. This value turns out to scatter between around a value of 1. We will compare these results with theoretical predictions for ideal nonwovens further below.

A key feature of the nonwoven considered so far was that it was composed of unimodal nanofibers i.e. with just one average diameter and that the fibers had a circular cross-sectional shape. In the following nonwovens are considered which are either characterized by a bimodal diameter distribution or by fibers which are ribbon-shaped. The concept behind these studies is to find out how strongly such increasing nonidealities manifest themselves in nonwoven properties.

3.2. Nonwovens with a bimodal fiber diameter distributions composed of PAN fibers

Such nonwovens were prepared as described above and also published previously in the literature by using four different die/feeding systems in combination with two different polymer concentrations in the respective spinning solution [27]. The

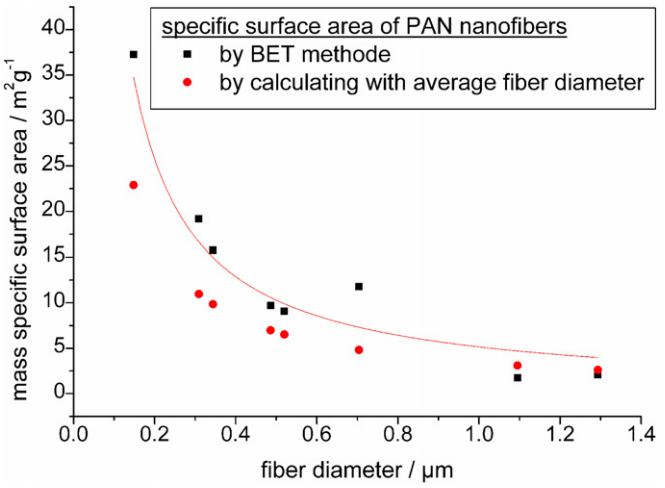

Fig. 6. Experimental data on the specific surface area as a function of the fiber diameters.

concentrations of the two spinning solutions – 9 w% and 14 w% in DMF – were chosen in such a way that the two fiber types were characterized by diameters of about 1700 and 400 nm respectively. The weight fractions of the two types of fiber diameters in the resulting nonwovens were controlled via the feeding rates selected for the four dies. Fig. 9 shows SEM-images for three nonwovens with different amounts of the two types of fibers.

We used the weight fraction of the two different fibers and their fiber diameter to define furthermore an effective fiber diameter (weight averaged diameter). This value is used in the following for comparisons of the data with those obtained for other types of nonwovens.. The total porosity turned out to correspond to the one found for nonwovens with unimodal fiber diameters, a value of 0.85 ± 0.02 was found.

The geometric pore sizes were determined from cross-sectional areas of imbedded nonwovens displayed in Fig. 10a as detailed in the experimental section. The cross-sections of the individual fibers with different diameters are readily evident in the image. The corresponding results shown in Fig. 10b relative to the weight

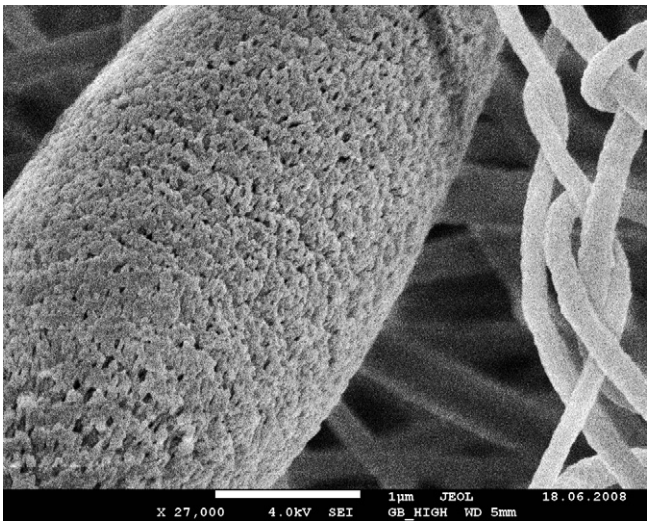

Fig. 7. Example for a nonideal surface of electrospun fibers such as caused by pores, surface roughness. Displayed is a fiber composed of PAN and spun from solution of PAN (7 w%) in DMF.

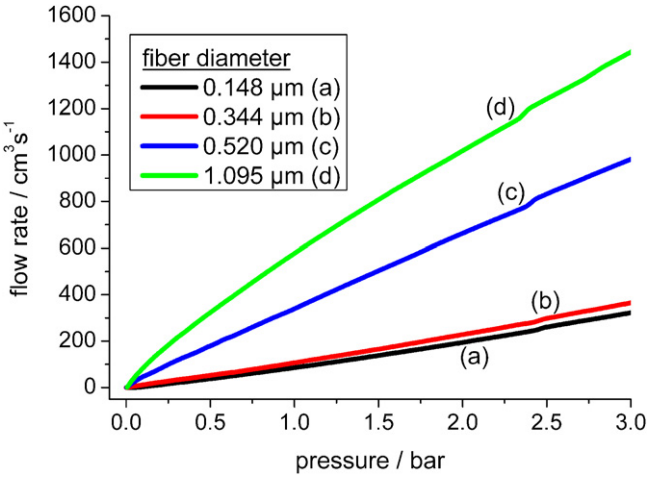

Fig. 8. Gas flow as function of pressure drop across the nonwovens (along *z*-axis, perpendicular to fiber planes) using the fiber diameter of PAN fibers as parameter.

averaged diameter show a linear relation between pore size and average fiber diameter as also found for the unimodal nonwovens. The ratio of the geometric pore size relative to the fiber diameter turns out to be about 6 again as in the case of nonwovens with unimodal fiber diameter distribution discussed above.

An interesting observation for capillary pore diameters as obtained by capillary flow porometry is obvious from Fig. 11a. The diameters of these pores stay about constant as the weight fraction of the thicker fibers increases from 0 up to about 60% and increase then very strongly with increasing fraction of the thicker fibers by more than a factor of 3. On the other hand using the weight averaged fiber diameter one observes an approximately increase of the pore diameters with increasing fiber diameter as obvious from Fig. 11b. The ratios of the diameters of the bubble point pores and the mean flow pores with respect to the averaged fiber diameters – i.e. roughly 6 and 9 respectively – correspond quite well to the ones observed for the nonwovens with unimodal fiber diameter distribution.

The investigations both on the specific surface area and on the permeation coefficient as a function of the averaged fiber diameter reveal that these values also correspond quite closely to the ones observed for nonwovens with unimodal fiber diameter distribution. A more detailed discussion can be found below.

3.3. Nanofiber nonwovens composed of nanofibers with ribbon-type geometry

It is well known from literature that electrospinning can give rise to flat fibers i.e. fibers with ribbon-like cross-sectional geometry for particular polymers and spinning solutions [8,11,15–17,31]. Polyamide 6 solved in formic acid is an example which will be considered in the following in some detail. Fibers with ribbon structures are available for polymer concentrations in the range from about between 27.5 and 32.5 w% with fiber dimensions in the range from about 500 up to about 2000 nm. The expectation is that this strong modification of the geometry of the fibers will indeed affect the nonwoven properties strongly. Fig. 12 shows a nonwoven containing such ribbon-type fibers.

First of all the observation with respect to the total porosity is that it decreases from a value of about 85% observed for nonwovens composed of fibers with circular cross-section to about 75% if the ribbon concentration amounts to 50%, the extrapolation yielding a total porosity of 68% for nonwovens composed purely of ribbon-type fibers. Variations in the geometry of the fibers obviously have a strong effect on the total porosity. The expectation thus is that pore sizes and permeation properties are also affected strongly by such change of geometry.

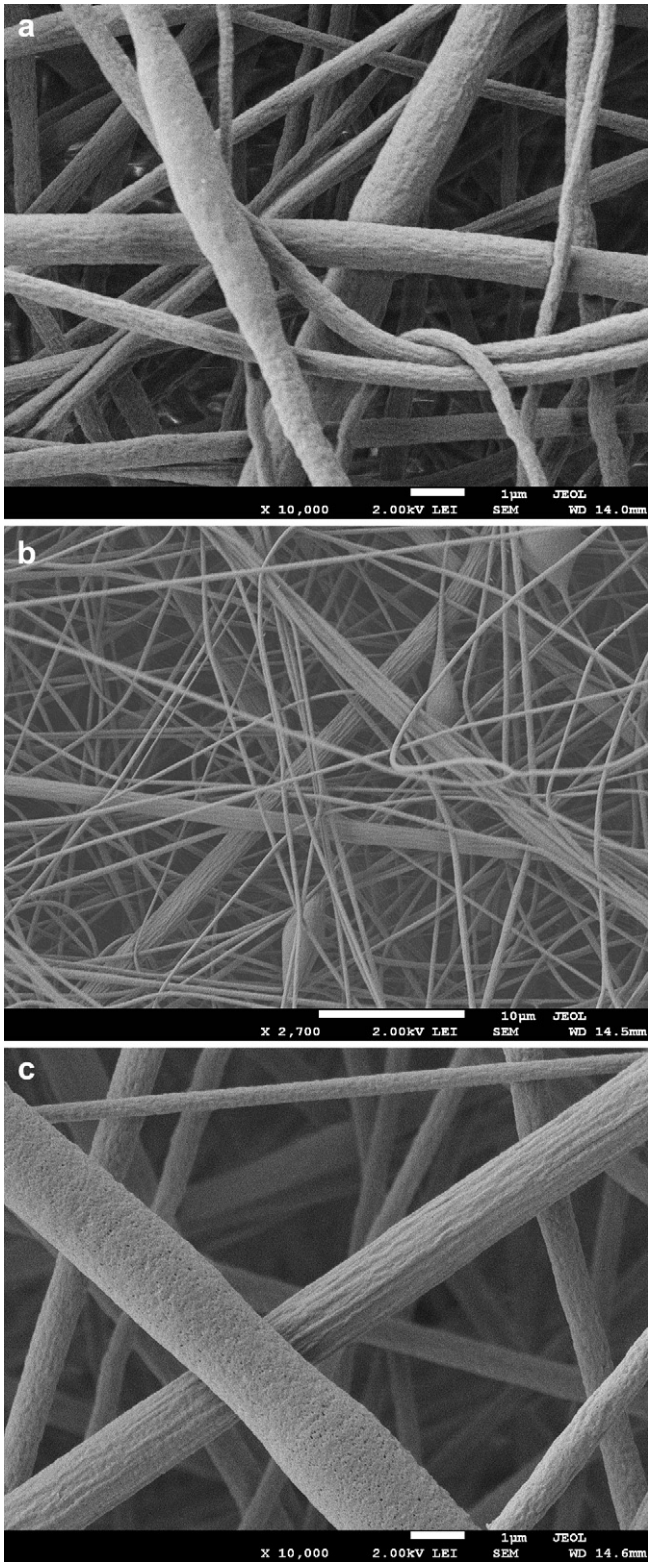

Fig. 9. Nonwovens composed of PAN fibers characterized by a bimodal fiber diameter distribution, composed of thicker fibers (1700 nm) and thinner fibers (400 nm). The weight fraction of thick fibers in the whole nonwoven amounts to a) 34%, b) 61%, c) 82%.

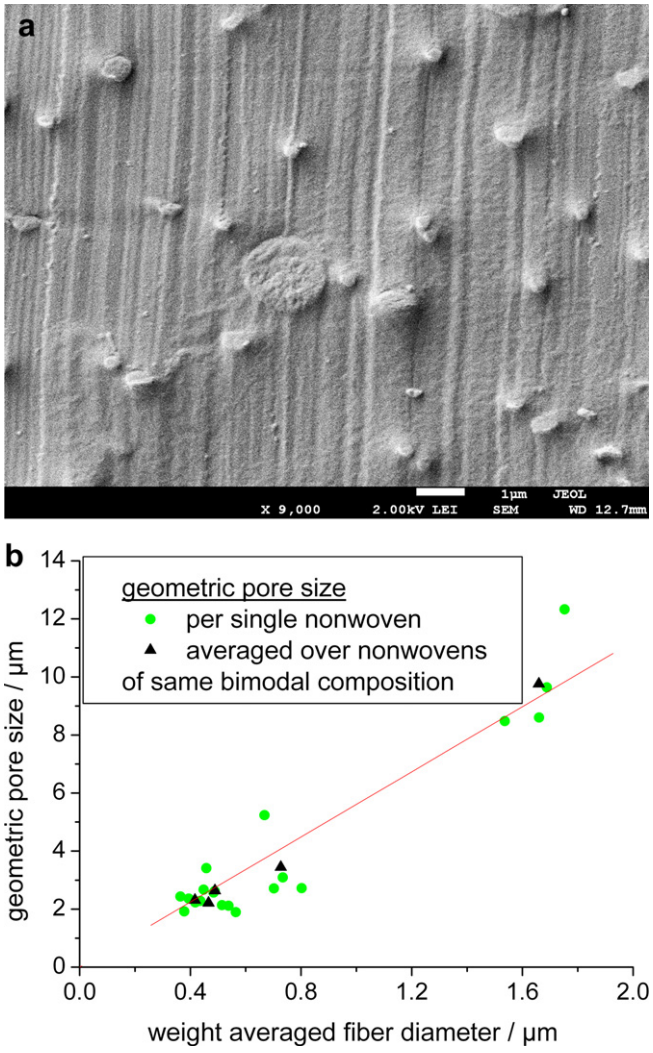

Fig. 10. a) Cross-sectional area of embedded nonwoven with bimodal fiber distribution, b) dependence of geometric pore sizes on weight averaged fiber diameter.

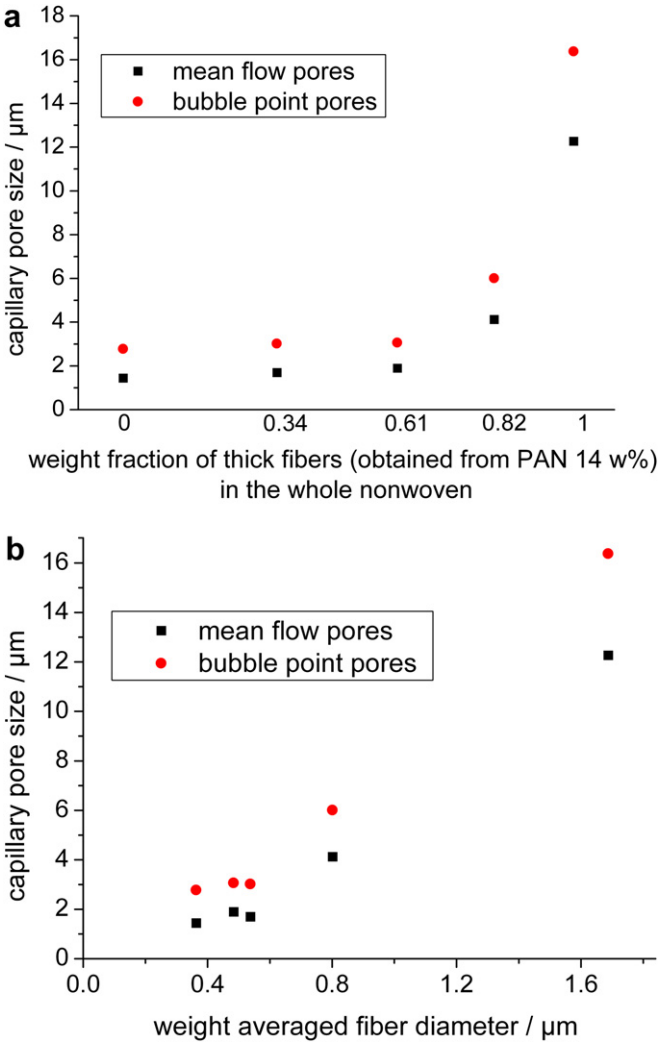

Fig. 11. Variation of the magnitudes of the capillary pore diameters a) with composition of the heterogeneous nonwoven, b) with the weight averaged fiber diameters.

In fact, the dimensions of the capillary pores are strongly reduced relative to the nonwovens considered so far. The ratios of the pore dimensions relative to the fiber dimensions (for the purpose of the comparison with the results reported above we have chosen the ribbon width as fiber diameter.) are reduced to 1 for the bubble point diameter and to about 0.5 for the average capillary pore diameter respectively as compared to 9 and 5 observed for the unimodal and bimodal nanofiber nonwovens. In a similar way the permeation coefficients are reduced by orders of magnitude in comparison to the ones observed for the unimodal and bimodal nanofiber nonwovens. They are of the order of 1×10^{-16} to 9×10^{-16} m^2.

The ribbon-type fibers cause quite obviously a different packing of the fibers within the nonwovens and they cause strong modifications in the flow process through the nonwovens. These results suggest that one can modify the structure and permeation properties over a broad range by preparing nonwovens with various concentrations of ribbon-type fibers. In fact ribbon-type fibers have also been reported for other types of polyamides, polycarbonate etc.

To learn more about the influences of fiber shape and fiber packing on the membrane properties it is helpful to compare the results described so far with model calculations considering both fiber diameters and packing parameters. This will be done below.

3.4. Real nonideal and ideal nanofiber nonwovens: comparison of experimental results and predictions

The experimental findings discussed so far showed that the permeation properties of electrospun nonwovens composed of fibers with a circular cross-section and with an unimodal diameter distribution or with a bimodal diameter distribution are to a good approximation identical and directly controlled by the respective average fiber diameters. The transition from fibers with a circular cross-section to ribbon-type fibers on the other hand induces strong modifications of the permeation properties. So the particular structure of a given electrospun nonwoven can have a significant impact on its permeation performance. To learn more about the effect of the particular structural features of electrospun nonwovens on these permeation properties it is instructive to compare the experimental results obtained for electrospun nonwovens with predictions on such properties for ideal nonwovens. These come predominantly from Monte Carlo simulations which will be briefly discussed in the following.

As already introduced above in these Monte Carlo simulations linear fiber segments with a given fiber diameter are deposited on a model plane one after the other [24–26]. Their individual orientations are chosen by various methods in such a way that

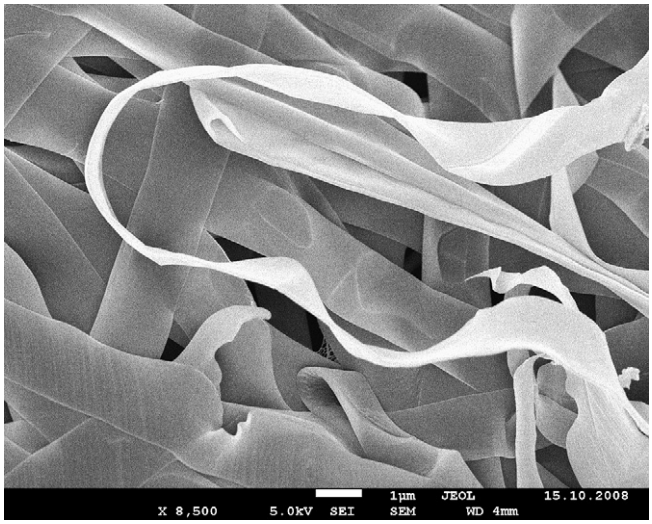

Fig. 12. Nonwovens containing ribbon-type fibers (PA 6 fibers, spun from 34 w% PA 6 in formic acid).

either planar isotropic or planar parallel arrangements result. Two types of fiber deposition modes are considered in these simulations namely nonoverlapping depositions or fully overlapping depositions. The fibers may touch each other at their surfaces in the first case whereas they are allowed to intersect each other in the second case sharing thus the same volume at certain contact locations. The key factor of such simulations, as far as predictions on structure property correlations in electrospun nanofiber nonwovens is concerned, is that ideal model nonwovens are considered which may serve in the context of this paper as standard structure for comparison. They are characterized by strictly linear fibers with uniform diameter and smooth surfaces are considered. Predictions on nonwoven structure property correlations are available from these simulations using the fiber diameter and the total porosity as they key structural parameters [24–26].

To make predictions on the pore dimensions the mean interception length $\overline{d}$ is analyzed as representation of the pore diameter. The interception length considered here represents the length of a linear segment oriented in a given way which fits just into a pore bordered by the nanofibers. The average is then taken with respect to all segment orientations and all positions in the nonwoven. Such a quantity can be taken as a good representation of the average linear dimension of a pore representing thus the geometric pore size. Furthermore such simulations allow to make predictions on the internal (volume) specific surface S in terms of the reduced quantity $S \times r$. [24–26]. These predictions again are in general expressed in terms of the reduced quantities i.e. relative to the fiber radius r.

The predictions can be represented by diagrams in which the reduced quantities (reduced relative to the fiber radius) are plotted versus the total porosity as shown in Fig. 13a and b for the pore dimensions and the specific surface area. In a similar way predictions on the peculiar permeation coefficients characteristic of the flow of gases, fluids through a nonwoven composed of nanofibers can be represented in a similar way [25,32] as shown in Fig. 13c.

The advantage of this comparison is that the role of different total porosities is actually taken into account. The results for real nonwovens composed of fibers with circular cross-sectional areas are that depending of the kinds of pore type considered – i.e. geometric or capillary ones- their sizes are rather close to the ones

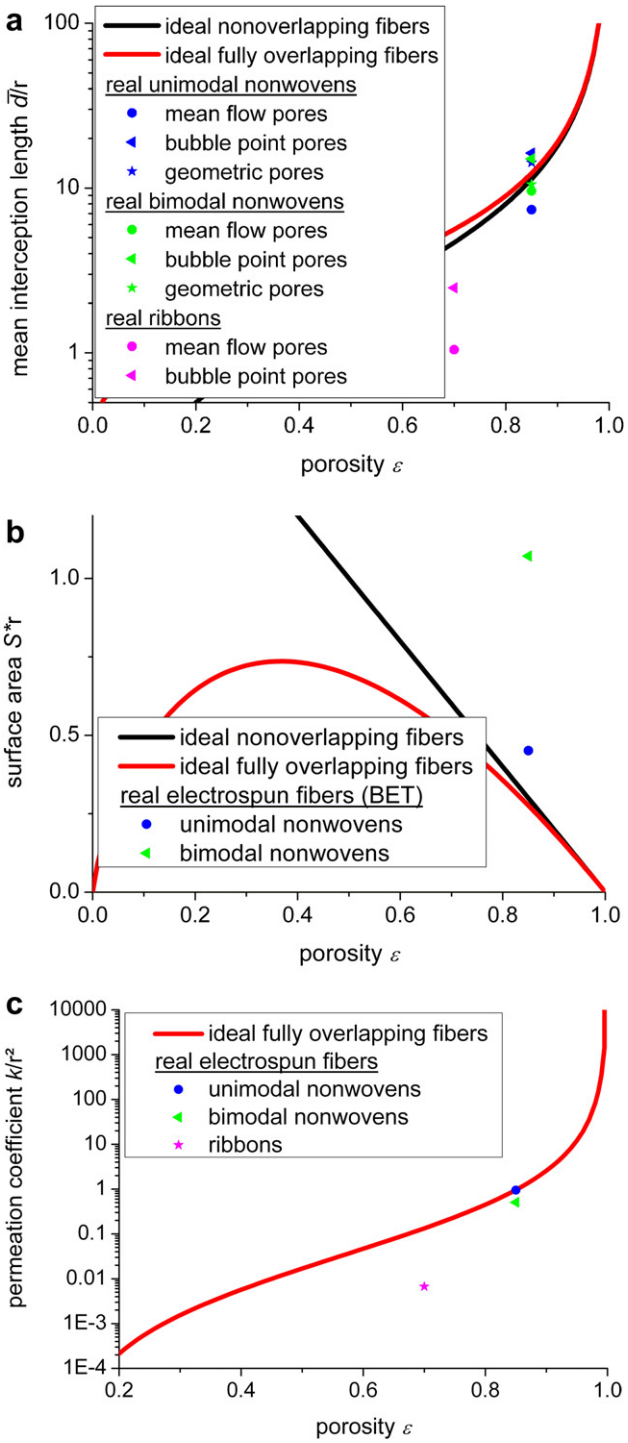

Fig. 13. Comparisons between experimental results for the different types on nonwovens considered here with predictions on ideal nonwoven structures a) pores sizes, b) specific surface area, c) permeation coefficients (Note that reduced quantities are considered in the theoretical curves with the fiber radius r being used for the reductions).

of ideal nonwoven with deviations being smaller than a factor of 2. Yet much stronger differences are found for ribbon-type fibers. Here the pore dimensions are smaller by more than one order of magnitude relative to the ones of ideal nonwovens. In the case of the permeation coefficients it is observed that they are on the average very similar for ideal and real nonwovens if fibers with circular cross-sectional areas are considered but about two orders

of magnitude lower for ribbon-type fibers. Finally the specific surface areas tend to be larger than the predicted ones for the ideal nonwovens ones with a factor of about 2 being found for the bimodal system. It seems that surface structures of the type shown in Fig. 7 of the fibers contribute to this increase.

It has thus become obvious that the nonideal structures characteristic of electrospun nonwovens manifest themselves in membrane properties such as pore sizes, specific surfaces and permeation coefficients in very specific ways.

4. Conclusion

A detailed knowledge on characteristic nonwoven properties such as pore sizes, including geometric pore sizes as well as capillary pore sizes responsible for the control of permeation, the specific surface and finally permeation coefficients is a must as far as dedicated design and preparation of such nonwovens for particular applications – filters, textiles, scaffolds for tissue engineering, carrier for catalysts – is concerned. Yet such a detailed knowledge has been missing in the literature to a large extent in particular as far as nanofiber nonwovens as produced by electrospinning are concerned. From the experimental results discussed above it has become obvious, first of all, that experimental methods are available allowing to characterize all these nonwoven properties in detail and to correlate them to structural properties of the nonwovens such as fiber diameters, porosity and nonwoven architecture. These, in turn, can be controlled by electrospinning parameters so that one is able to adjust the spinning parameters closely to come up with the target nonwoven properties.

In the present contribution we have additionally looked briefly at predictions on nonwoven structure property correlations coming from Monte Carlo simulations on ideal nonwovens. This allowed to get some insights into the role of nonideal structures resulting from electrospinning on permeation properties. Conclusions are first of all that the nonideal structures characteristic of electrospun nonwovens manifest themselves in membrane properties such as pore sizes, specific surfaces and permeation coefficients in very specific ways and secondly that in general the effects of nonideal structural features are limited in magnitude as long as fibers with circular cross-sectional areas are concerned whereas strong modifications occur for ribbon-type nanofibers.

Acknowledgements

We gratefully acknowledge the support by Dr. Andreas Schaper and Martin Hellwig in helping us to obtain the SEM images and by Prof. Kissel (Department of Pharmacy, Marburg) and his group for the BET analysis.

References

[1] Dersch R, Greiner A, Wendorff JH. In: Schwartz JA, Contesen CJ, Putger K, editors. Dekker encyclopedia of nanoscience and nanotechnology. New York: Marcel Dekker; 2004. p. 2931.
[2] Li D, Xia Y. Adv Mater 2004;16:1151.
[3] Greiner A, Wendorff JH. Angew Chem Int Ed 2007;46:5670.
[4] Reneker DH, Yarin AL, Zussman E, Xu H. Adv Appl Mechanics 2007:41–4.
[5] Ramakrishna S. An introduction to electrospinning and nanofibers. New Jersey: World Scientific Pub.; 2005.
[6] Huang ZM, Zhang YZ, Kotaki M, Ramakrishna S. Composites Sci Technol 2003;63:2223.
[7] Teo WE, Ramakrishna S. Nanotechnology 2006;17:R89.
[8] Greiner A, Wendorff JH. Adv Polym Sci 2008;219:107.
[9] Bognitzki M, Czado W, Frese T, Schaper A, Hellwig M, Steinhart M, et al. Adv Mater 2001;13:70–2.
[10] Casper CL, Stephens JS, Tassi NG, Chase DB, Rabolt JF. Macromolecules 2004;37:573–8.
[11] Megelski S, Stephans JS, Bruce CD, Rabolt JF. Macromolecules 2002;35:8456–66.
[12] Li D, Ouyang G, McCann JT, Xia Y. Nano Lett 2005;5:913–6.
[13] Hellen EKO, Alava MJ, Niskanen KJ. J Appl Phys 1997;81:6425–31.
[14] Holzmeister A. Diplomarbeit. Philipps-Universität Marburg; 2006.
[15] Huang CB, Chen SL, Lai CL, Reneker DH, Qiu H, Ye Y, et al. Nanotechnology 2006;17:1558.
[16] Shkadov VY, Shutov AA. Fluid Dyn Res 2001;28:23.
[17] Koombhongse S, Liu WX, Reneker DH. J Polym Sci Part B-Polymer Phys 2001;39:2598.
[18] Placke D. PhD Thesis, Philipps University, Marburg; 2007.
[19] Boland ED, Wnek GE, Simpson DG, Palowski KJ, Bowlin GL. J Macromol Sci Pure Appl Chem 2001;38:1231–43.
[20] Zussman E, Theron A, Yarin AL. Appl Phys Lett 2003;82:973–5.
[21] Fong H, Reneker DH. Hanser, München. In: Salem DR, editor. Structure formation in polymeric fibers; 2001. p. 225–46.
[22] Dersch R, Liu T, Schaper AK, Greiner A, Wendorff JH. J Polym Sci Part A 2003;41:545–53.
[23] A. Holzmeister, A. Greiner, J.H. Wendorff. Polym Eng Sci; 49(Suppl. 1): 148–53.
[24] Tomadakis MM, Sotirchos SV. AIChE J 1991;37:1175.
[25] Tomadakis MM, Robertson TJ. J Compos Mater 2005;39:163.
[26] Tomadakis MM, Sotirchos SV. AIChE J 1991;37:74.
[27] Holzmeister A, Rudisile M, Greiner A, Wendorff JH. Europ Polym J 2007; 43:4859.
[28] Jena A, Gupta K. Fluid Part Separat J 2002;4:227.
[29] Jena A, Gupta K. Int Wovens J 2005;26.
[30] Brunauer S, Emmett PH, Teller E. J Am Chem Soc 1938;60:309.
[31] A. Holzmeister. Diplomarbeit, Marburg; 2006.
[32] Johnson DL, Koplik J, Schwartz LM. Phys Rev Lett; 1986:572564.